

Photon echoes retrieved from semiconductor spins: access to basis for long-term optical memories

L. Langer,¹ S.V. Poltavtsev,^{1,2} I.A. Yugova,² M. Salewski,¹ D.R. Yakovlev,^{1,3}
G. Karczewski,⁴ T. Wojtowicz,⁴ I.A. Akimov,^{1,3} and M. Bayer¹

¹Experimentelle Physik 2, Technische Universität Dortmund, 44221 Dortmund, Germany

²Spin Optics Laboratory, Saint Petersburg State University, 198504 St. Petersburg, Russia

³A.F. Ioffe Physical-Technical Institute, Russian Academy of Sciences, 194021 St. Petersburg, Russia

⁴Institute of Physics, Polish Academy of Sciences, PL-02668 Warsaw, Poland

The possibility to store optical information is important for classical and quantum communication. Atoms or ions as well as color centers in crystals offer suitable two-level systems for absorbing incoming photons. To obtain a reliable transfer of coherence, strong enough light-matter interaction is required, which may enforce use of ensembles of absorbers, but has the disadvantage of unavoidable inhomogeneities leading to fast dephasing. This obstacle can be overcome by echo techniques that allow recovery of the information as long as the coherence is preserved. Albeit semiconductor quantum structures appear appealing for information storage due to the large oscillator strength of optical transitions, inhomogeneity typically is even more pronounced for them and most importantly the optical coherence is limited to nanoseconds or shorter. Here we show that by transferring the information to electron spins the storage times for the optical coherence can be extended by orders of magnitude up to the spin relaxation time. From the spin reservoir it can be retrieved on purpose by inducing a stimulated photon echo. We demonstrate this for an n-doped CdTe/(Cd,Mg)Te quantum well for which the storage time thereby could be increased by more than three orders of magnitude from the picosecond-range up to tens of nanoseconds.

Photon echoes are amazing optical phenomena in which resonant excitation of a medium by short optical pulses results in a delayed response in form of a coherent optical flash. Since their first observation in ruby in 1964 [1], photon echoes were reported for atom vapors [2], rare earth crystals [3] and semiconductors [4, 5]. Spontaneous (two-pulse) and stimulated (three-pulse) photon echoes were demonstrated and used for studying the involved energy levels and the coherence evolution of the optical transitions [6, 7, 8]. Currently there is great interest in application of photon echoes for quantum memories [9, 10]. Photon echoes occur in an ensemble of oscillators with an inhomogeneous distribution of optical transitions. Such an ensemble provides high efficiency and large bandwidth allowing one to

store multiple photons with high capacity. Current activities on photon echoes have mainly concentrated on rare earth crystals and atomic vapors with long storage times, that are crucial for implementation of robust light-matter interfaces.

Already at the early stage of photon echo experiments the spin level structure of ground and excited states was recognized to contribute to the formation of spontaneous and stimulated photon echo signals [11, 12, 13]. If optically addressed states possess orbital and/or spin angular momenta then the splitting of these states by a magnetic field (the Zeeman effect) provides an additional degree of freedom for the control of photon echo through optical selection rules [14, 15, 16]. Moreover, transfer of coherence from optical to spin excitations has been suggested to considerably extend the storage times as demonstrated for quasi-atomic systems having optical and spin coherences with comparable lifetimes [17]. Here we demonstrate that a transverse magnetic field applied to a semiconductor leads to transfer of short-lived optical coherence into long-lived electron spin coherence. This allows one to induce stimulated photon echoes on sub- μ s time scales, exceeding the radiative lifetime of the optical excitations by more than three orders of magnitude. We reveal two mechanisms leading to this extension of stimulated echo revival - coherence transfer and spin fringes, and show that depending on the polarization configuration of the three involved laser pulses we are able to shuffle the optical coherence into a spin component that is directed either along or perpendicular to the magnetic field. The spins directed along magnetic field are free of any dephasing and are affected little by spin relaxation, which makes this configuration highly appealing for future applications in memory devices.

For demonstration of magnetic-field-induced stimulated photon echoes, we study a semiconductor CdTe/(Cd,Mg)Te quantum well (QW) which serves as model system, that can be tailored for the targeted application on a detailed level by nanotechnology. The fundamental optical excitations in semiconductors, the excitons, possess large oscillator strength so that resonant absorption may be achieved with close to unity efficiency even for structure thicknesses smaller than the light wavelength. Therefore propagation effects are not as important as in atomic vapors and rare-earth crystals.

Ultrafast coherent spectroscopy of excitons employing laser pulses is well established for semiconductor nanostructures [7]. However, for storage applications excitons have been scarcely considered because of their limited optical coherence time T_2 due to complex many body interactions and their short radiative lifetime ($T_1 \leq 1$ ns) being the downside of the large oscillator strength. In nanostructures such as quantum dots (QDs) the optical decoherence is weak but still limited by radiative decay. Therefore approaches to involve the long-lasting coherence of electron spins have been pursued recently where most of the studies were focused on optical control of the spin [18, 19, 20, 21]. The storage and retrieval of optical coherence by its encoding in an ensemble of electron spins has not yet been addressed.

Figure 1 summarizes the experimental approach and the main results on the optical properties of the studied QW in zero magnetic field. We use a sequence of three excitation pulses with variable delays τ_{12} between pulses 1 and 2 and τ_{23} between pulses 2 and 3. The duration of the pulses $\tau_p \approx 2 \div 3$ ps. Pulses 2 and 3 are propagating along the same direction, so that their wave vectors are equal $\mathbf{k}_2 = \mathbf{k}_3$. Both the spontaneous (PE) and stimulated (SPE) photon echoes are then directed along the $2\mathbf{k}_2 - \mathbf{k}_1$ direction. The transients are measured by taking the cross-correlation of the resulting four-wave mixing signal $E_{\text{FWM}}(t)$ with the reference pulse $E_{\text{ref}}(t)$ using heterodyne detection as schematically shown in

Fig. 1A [see appendix A]. This allows us to distinguish between the PE and SPE signals because of their different arrival times at the detector.

Essential for our experiment is selection of a well-defined spin level system, optically excitable according to clean selection rules. That is why we did not select the neutral exciton but the charged exciton consisting of two electrons and a hole, which requires a resident electron population. The studied sample comprises 20-nm thick CdTe QWs separated by 110 nm $\text{Cd}_{0.78}\text{Mg}_{0.22}\text{Te}$ barriers. The barriers are doped with donors which provide resident electrons for the QWs with density $n_e \approx 10^{10} \text{ cm}^{-2}$. At the cryogenic temperature of 2 K in experiment these electrons become localized in QW potential fluctuations due to well width and composition variations [22]. In the photoluminescence spectrum both the neutral (X) and charged exciton (in short, trion T^-) are observed, separated by the trion binding energy [23]. In the T^- ground state the two electrons form a spin singlet state. The narrow widths of the spectral lines indicate a high structural quality (see Fig. 1B).

To address solely the optical transition from electron to trion, the photon energy of the laser is tuned to the lower energy flank of the trion emission line, namely to $\hbar\omega = 1.599 \text{ eV}$. Thereby we also selectively excite T^- complexes with enhanced localization, having longer optical coherence time. The laser spectrum is shown by the dashed line in Fig. 1B. Figure 1C gives the characteristic four-wave mixing signal taken for $\tau_{12} = 23 \text{ ps}$ and $\tau_{23} = 39 \text{ ps}$, while the delay τ_{ref} of the reference pulse is scanned relative to pulse 1. Signatures of spontaneous (PE) and stimulated (SPE) photon echoes are clearly seen in the transients: the PE signal appears at $\tau_{\text{ref}} = 2\tau_{12}$ and the SPE shows up at $\tau_{\text{ref}} = 2\tau_{12} + \tau_{23}$ [6]. The decay of the PE and SPE peak amplitudes with increasing τ_{12} and τ_{23} , respectively, are shown in Fig. 1D. From these data we evaluate decay times of $T_2 = 72 \text{ ps}$ and $T_1 = 45 \text{ ps}$ so that $T_2 \approx 2T_1$ indicating that the loss of coherence for the trions is mainly due to radiative decay with lifetime $\tau_r = T_1$.

The investigated electron-trion transition can be considered as four-level system, as shown schematically in Fig. 2 [24]. We excite optical transitions between the doubly degenerate electron states with spin projections $S_z = \pm 1/2$ (ground states $|1\rangle$ and $|2\rangle$) and the doubly degenerate trion states with spin projections $J_z = \pm 3/2$ (excited states $|3\rangle$ and $|4\rangle$). The excited state spin projections are determined by the heavy-hole total angular momentum because the trion electrons form a singlet state ($S = 0$). The selection rules for optical excitation follow from angular momentum conservation, i.e. $|1\rangle + \sigma^+ \rightarrow |3\rangle$ and $|2\rangle + \sigma^- \rightarrow |4\rangle$ [25]. Here σ^+ and σ^- denote the corresponding circular photon polarizations. At zero magnetic field the transitions are decoupled. In addition, the spin relaxation time of hole T_h and electron T_e are long compared to the radiative lifetime ($T_e, T_h \gg \tau_r$) [22]. Therefore the SPE signal is expected to decay with $T_1 = \tau_r$ when the delay τ_{23} is increased, in full accord with the experimental data in Fig. 1D.

Application of an external magnetic field in the QW plane, $\mathbf{B} \parallel x$, leads to Larmor precession of the electron spin in the ground state. In that way the transfer of optical coherence into long-lived electron spin coherence can be achieved and a dramatic increase of the SPE decay time by several orders of magnitude may be accomplished. There are two different mechanisms which contribute to magnetic-field-induced signal (see Fig. 2). The first one (A) is based on direct transfer of optical coherence into electron spin coherence, and the second one (B) is due to de-synchronization of the spectral gratings for electron and trion spins.

For simplicity, let us consider a situation when the pulse duration τ_p is significantly shorter than the period of Larmor precession $T_L = 2\pi/\omega_L = 2\pi\hbar/g\mu_B B$, where g is the electron g -factor and μ_B is the Bohr magneton. Under these conditions the selection rules for optical transitions remain unchanged. For the mechanisms (A) and (B) it is important that the Larmor precession frequencies of the trion and electron spins are different. This is perfectly well the case in QW structures where the confinement along z direction splits the heavy-hole and light-hole bands and therefore the optically excited trion states do not become coupled by the weak transverse magnetic field because the transverse heavy-hole g -factor $g_{hh} \approx 0$ [26]. This feature simplifies analysis of the system's time evolution because one has to account only for Larmor precession of the electron spin, i.e. a periodic exchange between S_y and S_z with frequency ω_L . Also for simplicity, we consider the following relations between the time constants representing realistically the situation for the studied electron-trion system and corresponding as well to the most interesting case of long-lived echoes:

$$T_L \leq \tau_{12} \ll T_2, \quad (1)$$

$$T_1 \ll \tau_{23} \ll T_e \text{ and } T_1 \ll T_h. \quad (2)$$

The first relation requires fast Larmor spin precession and conservation of optical coherence before arrival of pulse 2. The second relation limits our consideration to arrival times of pulse 3 after trion recombination, i.e. the system is in the ground state at $t = \tau_{23}$ and all required information is stored in the electron spin. Here we remind that $\tau_r \approx T_1 \approx T_2/2$. If relations 1 and 2 hold the solutions of the Lindblad equation of motion for the (4×4) density matrix ρ_{ij} , which describes the four-level electron-trion system, can be written in a compact form. For the electron spin components containing the required terms with $\exp(-i\omega_0\tau_{12})$ time evolution (see appendix B) we obtain:

$$S_x = \frac{\rho_{12} + \rho_{21}^*}{2} \propto K\Sigma \sin\left(\frac{\omega_L\tau_{12}}{2}\right) \exp\left(-\frac{\tau_{23}}{T_1^e}\right), \quad (3)$$

$$S_y = \frac{\rho_{12} - \rho_{21}^*}{2i} \propto K\Delta \sin\left(\frac{\omega_L\tau_{12}}{2} + \omega_L\tau_{23}\right) \exp\left(-\frac{\tau_{23}}{T_2^e}\right), \quad (4)$$

$$S_z = \frac{\rho_{11} - \rho_{22}}{2} \propto -K\Delta \cos\left(\frac{\omega_L\tau_{12}}{2} + \omega_L\tau_{23}\right) \exp\left(-\frac{\tau_{23}}{T_2^e}\right). \quad (5)$$

Here $K = \exp[-i(\omega_0\tau_{12} - \mathbf{k}_1\mathbf{r} + \mathbf{k}_2\mathbf{r})] \exp(-\tau_{12}/T_2) + c.c.$ is the term that carries the information on the optical phase, $\Delta = \theta_{1+}\theta_{2+} - \theta_{1-}\theta_{2-}$ and $\Sigma = \theta_{1+}\theta_{2+} + \theta_{1-}\theta_{2-}$ account for σ^\pm light polarization of the excitation pulse n with pulse area $\theta_{n\pm} \ll 1$. T_1^e and T_2^e correspond to the longitudinal and transverse electron spin relaxation times, respectively. ω_0 is the trion resonance frequency. Here we assume that initially, before the arrival of pulse 1 ($t < 0$), the electron spins are unpolarized, i.e., $\rho_{11} = \rho_{22} = 1/2$, while all other elements of the density matrix vanish. From equations 3-5 it follows that at $B > 0$ all spin components are finite with magnitudes depending critically on the polarization of the exciting pulses.

Qualitatively the magnetic-field-induced SPE evolution is easy to follow for a circular polarized pulse sequence as shown in Fig. 2. At $t = 0$ pulse 1 creates a coherent superposition between the states $|1\rangle$ and $|3\rangle$. This is an optical coherence associated with the ρ_{13} element of the density matrix. Due

to inhomogeneous broadening of optical transitions, this coherence ρ_{13} disappears due to dephasing. Each dipole in the ensemble with a particular optical frequency ω_0 acquires an additional phase $\phi(t) = (\omega - \omega_0)t = \delta\omega_0 t$ before arrival of the second pulse at $t = \tau_{12}$ (see term K in Eqs. 3-5). This is indicated by a set of arrows with different lengths, symbolizing the phase distribution of the dipoles with different frequencies.

The first mechanism (A) (see Fig. 2A) is most efficient when the second pulse arrives at $\tau_{12} = (2m + 1)\pi/\omega_L$, where m is an integer, i.e. the optical coherence ρ_{13} is shuffled into a ρ_{23} coherence between the optically inaccessible states $|2\rangle$ and $|3\rangle$. Pulse 2 transfers this coherence into a superposition of states $|1\rangle$ and $|2\rangle$, corresponding to spin coherence $\rho_{12} = S_x - iS_y$ (see Eqs. 3 and 4). There the coherence is frozen in the ground state without any further optical dephasing and can survive for much longer times than the zero-field coherence, even after radiative trion recombination τ_r . Note, however, that the Larmor precession of the electron spin is continuing then. Therefore dephasing of the S_y component may occur, while S_x remains constant as it is directed along the magnetic field (see Eqs. 3 and 4). Finally, pulse 3 retrieves the coherence ρ_{12} by converting it back into the optical frequency domain and starting the rephasing process. Again, the rephasing will be most efficient if $\rho_{12}(t = \tau_{12} + \tau_{23}) = \rho_{12}^*(t = \tau_{12})$, i.e. for $\tau_{23} = (2l + 1)\pi/\omega_L$, where l is an integer.

The second mechanism (B) (see Fig. 2B) can be considered as an incoherent one. In contrast to the first one it relies on population rather than coherence. Here, the accumulated phase of each dipole ϕ is projected by pulse 2 into population interference fringes $\rho_{11} \propto \sin^2(\delta\omega_0\tau_{12}/2)$ and $\rho_{33} \propto \cos^2(\delta\omega_0\tau_{12}/2)$, i.e. into spectral population gratings in the excited and ground states with opposite phase [6]. They are equivalent to spectral spin gratings for the electrons $S_z = (\rho_{11} - \rho_{22})/2$ and the trions $J_z = (\rho_{33} - \rho_{44})/2$. In contrast to the previous mechanism the interference fringes have the highest contrast when the second pulse arrives after an integer number of electron spin revolutions $t = \tau_{12} = 2m\pi/\omega_L$ (see Eq. 5). For $t > \tau_{12}$ the Larmor precession of the electron spin de-synchronizes the spin gratings in ground and excited state. Therefore even after trion recombination the electron spin grating does not disappear. The spin fringes $S_z(\delta\omega_0)$ and $J_z(\delta\omega_0)$ are schematically shown in Fig. 2C,D for two different times: the time of their creation $t = \tau_{12}$ and the time after trion recombination before arrival of pulse 3. Accordingly a long-lived electron spin grating is present, allowing one to retrieve the phase information ϕ and observe the SPE pulse with maximum signal at $\tau_{23} = l\pi/\omega_L$.

In practice, the initial condition of zero electron spin polarization is hard to match for circularly polarized pulse sequences. This is because σ^+ excitation induces a macroscopic spin polarization. The electron spin relaxation $T_2^e \sim 30$ ns is longer than the pulse repetition period $T_R = 13.2$ ns in our experiment and $\mathbf{S}(t = 0) \neq 0$ [22]. Moreover, for arbitrary τ_{12} , both mechanisms are present and therefore all spin components contribute to the SPE signal. Therefore circularly polarized pulses are not optimal for demonstration of magnetic-field-induced SPE. From Eqs. 3-5 it follows that a linearly polarized pulse sequence is much more attractive. For linearly $H = (\sigma^+ + \sigma^-)/\sqrt{2}$ or $V = (\sigma^+ - \sigma^-)/\sqrt{2}$ co-polarized pulses, $\Delta = 0$ and $\Sigma = 2\theta_1\theta_2$ so that only the dephasing-free S_x component is involved. Here we exploit only the first mechanism (A) of coherence transfer. If the pulses 1 and 2 are cross-polarized the opposite situation with $\Delta = 2\theta_1\theta_2$ and $\Sigma = 0$ is obtained. Here, the S_y and S_z

components contribute. The corresponding SPE amplitudes are given by

$$P_{HHHH} \propto \sin^2 \left(\frac{\omega_L \tau_{12}}{2} \right) \exp \left(-\frac{\tau_{23}}{T_1^e} \right) \quad (6)$$

$$P_{HVVH} \propto \cos [\omega_L (\tau_{12} + \tau_{23})] \exp \left(-\frac{\tau_{23}}{T_2^e} \right), \quad (7)$$

where the polarization sequence is denoted by the subscript ABCD with A, B, C corresponding to the polarizations of pulses 1, 2, 3, respectively, and D is the polarization of the resulting SPE pulse (see appendix B). Note that the SPE echo in HVVH configuration oscillates with the Larmor precession frequency in dependence of $\tau_{12} + \tau_{23}$, while in HHHH configuration it varies only with the τ_{12} delay time. Also the decay of the signals is different. For HVVH the decay occurs according to the transverse spin relaxation time T_2^e and additional dephasing due to the electron g-factor inhomogeneity Δg may play a role. In HHHH the signal decays with the longitudinal spin relaxation time T_1^e .

The experimental data for the SPE amplitude as function of delay time τ_{23} and magnetic field B , measured in the HHHH and HVVH polarization configurations, are summarized in Fig. 3. The delay time between pulses 1 and 2 is set to $\tau_{12} = 27$ ps, which corresponds to $T_L/\tau_{12} = 0.40$ at $B = 0.7$ T and $T_L/\tau_{12} = 0.086$ at $B = 0.15$ T. For comparison the SPE decay measured at $B = 0$ is shown in Fig. 3A. The magnetic field dependence of the SPE amplitude in Fig. 3B and 3D is measured for $\tau_{23} = 1.27$ ns which is significantly longer than the radiative lifetime T_1 . Note that the experimentally measured signal corresponds to the absolute value of amplitude $|P|$. In full accord with our expectations we observe a long-lived SPE signal when applying the magnetic field. The theoretical curves are in good agreement with the data. The calculations take into account the full dynamics of the system, including the excited states, and therefore reproduce also the short decay component of the SPE due to trion recombination as well as the signals at low magnetic fields with $T_L > \tau_{12}$ (see appendix B).

In case of HHHH no oscillations appear when τ_{23} is varied (see Fig. 3A), which is in line with Eq. 6. Particularly fascinating is the observation of SPE signal at negative delays ($\tau_{23} \sim -300$ ps) at a 75% level of the SPE amplitude at positive delays ($\tau_{23} \sim 300$ ps), see Fig. 3A. This means that within the pulse repetition period of 13 ns the SPE amplitude reduces by 25% only. From these data we estimate $T_1^e \sim 50$ ns, which allows us to observe SPE signals in magnetic field on a sub- μ s timescale. The short dynamics at negative delays -200 ps $< \tau_{23} < 0$ is due to excitation of trions by pulse 3, which influences the initial conditions at $t = 0$. Note that for the linearly polarized pulse sequence no macroscopic spin polarization becomes involved in the PE experiment due to inhomogeneous broadening of the optical transitions. Therefore we obtain information about the intrinsic longitudinal spin relaxation of the electron spin. The experimental data demonstrate that transfer of coherence to S_x is feasible and attractive because this spin component being parallel to \mathbf{B} is robust against relaxation and is not sensitive to dephasing. In contrast, the oscillatory signal in the HVVH polarization configuration decays much faster due to electron g-factor inhomogeneity and consequently no long-lived SPE signal is observed at negative delays (see Fig. 3C). The reduction of SPE signal at $B > 0.3$ T in Fig. 3D is also related to this fact. From fitting the data we evaluate $\Delta g = 0.018$.

In conclusion, we have demonstrated magnetic-field-induced long-lived stimulated photon echoes in

the electron-trion system. By a proper choice of polarization pulse sequence optical coherence can be transferred into spin directed along magnetic field. Although no metastable states are involved, due to the long-lived electron spin coherence, the timescale of echo stimulation can be extended by more than 3 orders of magnitude over the optical coherence time in the QW system. Note that the electron-trion energy level structure is identical in QWs and self-assembled quantum dots (QDs). We used QWs for demonstration purpose because the trion transitions are well isolated spectrally. As a downside, we had to keep the excitation power low in order to suppress many-body effects. In case of singly charged QD structures $\pi/2$ and π pulses can be efficiently used for coherent manipulation [27]. In addition the longitudinal spin relaxation times in, e.g., (In,Ga)As QDs may be as long as 0.1 s [28]. Further exploiting hyperfine interaction between electrons and nuclei might enable storage time of seconds or longer [29]. Therefore our findings open a new avenue for realization of optical memories in semiconductor nanostructures.

Acknowledgements

The Dortmund team would like to acknowledge financial support of this work by the Deutsche Forschungsgemeinschaft, the Bundesministerium für Bildung und Forschung (project Q.com-H). The project "SPANGL4Q" acknowledges the financial support of the Future and Emerging Technologies (FET) programme within the Seventh Framework Programme for Research of the European Commission, under FET-Open grant number: FP7-284743. S.V.P. and I.A.Yu. acknowledge partial financial support from the Russian Ministry of Science and Education (contract No.11.G34.31.0067). The research in Poland was partially supported by the National Science Center (Poland) under the Grants DEC-2012/06/A/ST3/00247 and DEC-2013/ST3/229756.

A Methods

The semiconductor quantum well (QW) structure was grown by molecular-beam epitaxy. It comprises 5 electronically decoupled 20 nm thick CdTe QWs embedded in 110 nm $\text{Cd}_{0.78}\text{Mg}_{0.22}\text{Te}$ barriers. The barriers are doped by iodine donors, which provide the QW layers with conduction band electrons of low density $n_e \sim 10^{10} \text{ cm}^{-2}$ [22]. The sample was mounted into a liquid He bath cryostat at a temperature of 2 K. Magnetic fields up to 0.7 T were applied in Voigt geometry using an electromagnet. The direction of the magnetic field was parallel to the QW plane ($\mathbf{B} \parallel x$).

We used tunable self mode-locked Ti:Sa laser as source of the optical pulses with durations of $2 \div 3$ ps at a repetition rate of 75.75 MHz (repetition period $T_R = 13.2$ ns). The laser was split into four beams. Three of them were used for the three pulse sequence required for stimulating the photon echo. The fourth beam was used as reference pulse in the heterodyne detection. The delay between all four pulses could be scanned by reflectors mounted on mechanical translation stages. The three-pulse four-wave mixing (FWM) experiment was performed in reflection geometry. Pulse 1 with wavevector \mathbf{k}_1 hit the sample under an incidence angle of about 7° . Pulses 2 and 3, both traveled along the same direction ($\mathbf{k}_2 = \mathbf{k}_3$) different from that of the first beam, hit the QW structure under an incidence angle of about 6° . The beams were focused onto the sample in a spot of about $200 \mu\text{m}$ in diameter. The intensities of each pulse were selected such as to remain in the linear excitation regime for each of the beams (pulse energy around $10\text{-}100 \text{ nJ/cm}^2$). The FWM signal was collected along the $2\mathbf{k}_2 - \mathbf{k}_1$ direction. We used interferometric heterodyne detection where the FWM signal and the reference beam are overlapped at a balanced detector [30]. The optical frequencies of pulse 1 and reference pulse were shifted by 40 MHz and 41 MHz with acousto-optical modulators. The resulting interference signal at the photodiode was filtered by a high frequency lock-in amplifier selecting $|2\omega_2 - \omega_1 - \omega_{\text{ref}}| = 1 \text{ MHz}$. This provided a high sensitivity measurement of the absolute value of the FWM electric field amplitude in real time when scanning the reference pulse delay time τ_{ref} , which was taken relative to the pulse 1 time arrival. The polarization of the first and the second pulses, as well as the detection polarization, were controlled with retardation plates in conjunction with polarizers.

B Theoretical description of magnetic-field-induced SPE

B.1 Stimulated photon echo in magnetic field

Let us consider optical excitation of the negatively charged trion by a short laser pulse with frequency ω close to the trion resonance frequency ω_0 . The incident electromagnetic field induces optical transitions between the electron state and the trion state creating a coherent superposition of these states. In accordance with the selection rules, σ^+ circularly polarized light creates a superposition of the $+1/2$ electron and $+3/2$ trion states, while σ^- polarized light creates a superposition of the $-1/2$ electron and $-3/2$ trion states. In order to describe these superpositions and the resulting dynamics in a magnetic field we use a 4×4 time-dependent density matrix, comprising the two electron spin projections ($\pm 1/2$) (index 1 and 2) and the two hole spin projections ($\pm 3/2$) (index 3 and 4).

The temporal evolution of the density matrix is described by the Lindblad equation:

$$\dot{\rho} = -\frac{i}{\hbar}[\hat{H}, \rho] + \Gamma. \quad (8)$$

Here \hat{H} is the Hamiltonian of the system and Γ describes relaxation processes phenomenologically. In our case the Hamiltonian contains three contributions: $\hat{H} = \hat{H}_0 + \hat{H}_B + \hat{V}$, where \hat{H}_0 is the Hamiltonian of the unperturbed spin system, \hat{H}_B gives the interaction with magnetic field and \hat{V} describes the interaction with light. In the calculations we use the short pulse approximation assuming that the pulse duration is significantly shorter than the trion lifetime, the decoherence times and the electron spin precession period in transverse magnetic field. This assumption is justified for our experimental conditions. Under these circumstances, we can separate and consider consistently the interaction of the electron-trion system with light and its dynamics in magnetic field.

B.2 Electron-trion system under action of short light pulse

The interaction with the electromagnetic wave in the electric-dipole approximation is described by the Hamiltonian:

$$\hat{V}(t) = - \int [\hat{d}_+(\mathbf{r})E_{\sigma+}(\mathbf{r}, t) + \hat{d}_-(\mathbf{r})E_{\sigma-}(\mathbf{r}, t)]d^3r, \quad (9)$$

where $\hat{d}_{\pm}(\mathbf{r})$ are the circularly polarized components of the dipole moment density operator, and $E_{\sigma\pm}(\mathbf{r}, t)$ are the correspondingly polarized components of the electric field of a quasi-monochromatic electromagnetic wave. The electric field of this wave is given by

$$\mathbf{E}(\mathbf{r}, t) = E_{\sigma+}(\mathbf{r}, t)\mathbf{o}_+ + E_{\sigma-}(\mathbf{r}, t)\mathbf{o}_- + \text{c.c.}, \quad (10)$$

where \mathbf{o}_{\pm} are the circularly polarized unit vectors that are related to the unit vectors $\mathbf{o}_x \parallel x$ and $\mathbf{o}_y \parallel y$ through $\mathbf{o}_{\pm} = (\mathbf{o}_x \pm i\mathbf{o}_y)/\sqrt{2}$. Here the components $E_{\sigma+}$ and $E_{\sigma-}$ contain temporal phase factors $e^{-i\omega t}$.

The strength of the light interaction with the electron-trion system is characterized by the corresponding transition matrix element of the operators $\hat{d}_{\pm}(\mathbf{r})$ calculated with the wave functions of the valence band, $|\pm 3/2\rangle$, and the conduction band, $|\pm 1/2\rangle$: [31]

$$d(\mathbf{r}) = \langle 1/2|\hat{d}_-(\mathbf{r})|3/2\rangle = \langle -1/2|\hat{d}_+(\mathbf{r})|-3/2\rangle. \quad (11)$$

We assume, that the trion recombination time is considerably shorter than the laser repetition period. Therefore, before the first pulse only elements of the density matrix describing the electron are unequal zero. We also assume, that these are only the populations ρ_{11} and ρ_{22} . Thus, the initial conditions are:

$$\rho(0) = \begin{pmatrix} \rho_{11}(0) & 0 & 0 & 0 \\ 0 & \rho_{22}(0) & 0 & 0 \\ 0 & 0 & 0 & 0 \\ 0 & 0 & 0 & 0 \end{pmatrix}. \quad (12)$$

The Hamiltonian $\hat{H} = \hat{H}_0 + \hat{V}$ in our basis is given by:

$$\frac{1}{2} \begin{pmatrix} 0 & 0 & f_+^* e^{i\omega t} \hbar & 0 \\ 0 & 0 & 0 & f_-^* e^{i\omega t} \hbar \\ f_+ e^{-i\omega t} \hbar & 0 & 2\hbar\omega_0 & 0 \\ 0 & f_- e^{-i\omega t} \hbar & 0 & 2\hbar\omega_0 \end{pmatrix}. \quad (13)$$

Here $f_{\pm}(t)$ is proportional to the smooth envelopes of the circular polarized components σ^+ and σ^- of the excitation pulse, given by

$$f_{\pm}(t) = -\frac{2e^{i\omega t}}{\hbar} \int d(\mathbf{r}) E_{\sigma_{\pm}}(\mathbf{r}, t) d^3r.$$

For simplicity we hereafter consider pulses with rectangular shape. This means that the pulse areas for the σ^{\pm} polarized components are equal to $f_{\pm}t_p$. In the experiment we investigate localized electrons and trions. We suppose, that the light wavelength is much larger than the length scale of localization. This allows one to extract the electric field $E_{\sigma_{\pm}}$ from the integral and write the pulse areas in the form $f_{\pm}t_p = \theta_{\pm}e^{i\mathbf{k}\mathbf{r}}$, where r is the position of the localized resident electron [32]. For calculations of the light-induced optical polarization and, therefore, the photon echo amplitude, we have to integrated the final expressions over the electron positions [32]. In experiment we operate in the linear regime of optical excitation of the QW, so that $|f_{\pm}t_p| \ll 1$ [33].

With these assumptions, the solution of the von Neumann equation $i\hbar\dot{\rho} = [\hat{H}_0 + \hat{V}, \rho]$ after the pulse action gives:

$$\begin{aligned} \rho_{11}^a &= \rho_{11}^b + \frac{it_p}{2}(f_+\rho_{13}^b - f_+^*\rho_{31}^b) + (\rho_{33}^b - \rho_{11}^b)\frac{|f_+t_p|^2}{4}, \\ \rho_{33}^a &= \rho_{33}^b - \frac{it_p}{2}(f_+\rho_{13}^b - f_+^*\rho_{31}^b) - (\rho_{33}^b - \rho_{11}^b)\frac{|f_+t_p|^2}{4}, \\ \rho_{22}^a &= \rho_{22}^b + \frac{it_p}{2}(f_-\rho_{24}^b - f_-^*\rho_{42}^b) + (\rho_{44}^b - \rho_{22}^b)\frac{|f_-t_p|^2}{4}, \\ \rho_{44}^a &= \rho_{44}^b - \frac{it_p}{2}(f_-\rho_{24}^b - f_-^*\rho_{42}^b) - (\rho_{44}^b - \rho_{22}^b)\frac{|f_-t_p|^2}{4}, \end{aligned} \quad (14a)$$

$$\begin{aligned} \rho_{13}^a &= e^{i\omega t_p}[\rho_{13}^b - \frac{if_+^*t_p}{2}(\rho_{33}^b - \rho_{11}^b) + \frac{f_+^*t_p^2}{4}(f_+\rho_{13}^b + f_+^*\rho_{31}^b)], \\ \rho_{24}^a &= e^{i\omega t_p}[\rho_{24}^b - \frac{if_-^*t_p}{2}(\rho_{44}^b - \rho_{22}^b) + \frac{f_-^*t_p^2}{4}(f_-\rho_{24}^b + f_-^*\rho_{42}^b)], \end{aligned} \quad (14b)$$

$$\begin{aligned} \rho_{14}^a &= e^{i\omega t_p}[\rho_{14}^b + \rho_{32}^b\frac{f_+^*f_-^*t_p^2}{4} + \frac{if_-^*t_p}{2}\rho_{12}^b - \frac{if_+^*t_p}{2}\rho_{34}^b], \\ \rho_{32}^a &= e^{-i\omega t_p}[\rho_{32}^b + \rho_{14}^b\frac{f_+f_-t_p^2}{4} + \frac{if_-t_p}{2}\rho_{34}^b - \frac{if_+t_p}{2}\rho_{12}^b], \end{aligned} \quad (14c)$$

$$\begin{aligned}
\rho_{12}^a &= \rho_{12}^b + \rho_{34}^b \frac{f_+^* f_- t_p^2}{4} + \frac{if_- t_p}{2} \rho_{14}^b - \frac{if_+^* t_p}{2} \rho_{32}^b, \\
\rho_{34}^a &= \rho_{34}^b + \rho_{12}^b \frac{f_+ f_-^* t_p^2}{4} + \frac{if_-^* t_p}{2} \rho_{32}^b - \frac{if_+ t_p}{2} \rho_{14}^b
\end{aligned} \tag{14d}$$

The superscripts ‘b’ and ‘a’ denote the matrix elements before and after pulse arrival, respectively.

B.3 Precession and relaxation in magnetic field

Next, we have to consider the dynamics in a transverse magnetic field. The magnetic field is applied perpendicular to the propagation direction of the incident light and to the structure growth axis. The corresponding Hamiltonian is:

$$\frac{1}{2} \begin{pmatrix} 0 & \hbar\omega_L & 0 & 0 \\ \hbar\omega_L & 0 & 0 & 0 \\ 0 & 0 & 2\hbar\omega_0 & \hbar\omega_L^T \\ 0 & 0 & \hbar\omega_L^T & 2\hbar\omega_0 \end{pmatrix}, \tag{15}$$

where ω_L and ω_L^T are the electron and trion Larmor precession frequencies. For simplicity we neglect the trion spin precession in magnetic field, i.e. $\omega_L^T = 0$, which is justified by the hole g-factor being close to zero.

Relaxation processes Γ are taken into account in the following way:

$$\begin{pmatrix} -\frac{\rho_{11}-\rho_{22}}{2T_z^e} + \frac{\rho_{33}}{\tau_r} & -\frac{\rho_{12}}{2T_s^e} - \frac{\rho_{21}}{2T_{s1}^e} & -\frac{\rho_{13}}{T_2} & -\frac{\rho_{14}}{T_2} \\ -\frac{\rho_{12}}{2T_{s1}^e} - \frac{\rho_{21}}{2T_s^e} & -\frac{\rho_{22}-\rho_{11}}{2T_z^e} + \frac{\rho_{44}}{\tau_r} & -\frac{\rho_{23}}{T_2} & -\frac{\rho_{24}}{T_2} \\ -\frac{\rho_{31}}{T_2} & -\frac{\rho_{32}}{T_2} & -\frac{\rho_{33}-\rho_{44}}{2T_s^h} - \frac{\rho_{33}}{\tau_r} & -\frac{\rho_{34}}{T_s^h} - \frac{\rho_{34}}{\tau_r} \\ -\frac{\rho_{41}}{T_2} & -\frac{\rho_{42}}{T_2} & -\frac{\rho_{43}}{T_s^h} - \frac{\rho_{43}}{\tau_r} & -\frac{\rho_{44}-\rho_{33}}{2T_s^h} - \frac{\rho_{44}}{\tau_r} \end{pmatrix}, \tag{16}$$

Here T_2 is the decay time of the optical coherence and τ_r is the trion recombination time. $\frac{1}{T_s^e} = \frac{1}{T_x^e} + \frac{1}{T_y^e}$, $\frac{1}{T_{s1}^e} = \frac{1}{T_x^e} - \frac{1}{T_y^e}$. $T_{x,y,z}^e$ are the electron spin relaxation times. Because the magnetic field points along the x axis, we assume $T_x^e \equiv T_1^e$ (longitudinal spin relaxation time) and $T_z^e = T_y^e \equiv T_2^e$ (transverse spin relaxation time). For the trion spin relaxation one can write down similar decay terms, but because of $\omega_L^T = 0$ we introduce only one the spin relaxation time T_s^h .

First, let us consider the dynamics of the non-diagonal terms of the density matrix in magnetic field. After pulse action these elements are:

$$\begin{aligned}
\rho_{13}(t) &= [\rho_{13}^a \cos(\omega_L(t-t_0)/2) - i\rho_{23}^a \sin(\omega_L(t-t_0)/2)]e^{(t-t_0)(i\omega_0-1/T_2)}, \\
\rho_{23}(t) &= [\rho_{23}^a \cos(\omega_L(t-t_0)/2) - i\rho_{13}^a \sin(\omega_L(t-t_0)/2)]e^{(t-t_0)(i\omega_0-1/T_2)}, \\
\rho_{24}(t) &= [\rho_{24}^a \cos(\omega_L(t-t_0)/2) - i\rho_{14}^a \sin(\omega_L(t-t_0)/2)]e^{(t-t_0)(i\omega_0-1/T_2)}, \\
\rho_{14}(t) &= [\rho_{14}^a \cos(\omega_L(t-t_0)/2) - i\rho_{24}^a \sin(\omega_L(t-t_0)/2)]e^{(t-t_0)(i\omega_0-1/T_2)}.
\end{aligned} \tag{17}$$

Here t_0 is the time after end of the pulse action.

It is convenient to describe the evolution of the other elements of the density matrix through the electron and trion spin dynamics. Obviously the following relations hold:

$$\begin{aligned} S_z &= (\rho_{11} - \rho_{22})/2, & S_y &= i(\rho_{12} - \rho_{21})/2, & S_x &= (\rho_{12} + \rho_{21})/2, \\ J_z &= (\rho_{33} - \rho_{44})/2, & J_y &= i(\rho_{34} - \rho_{43})/2, & J_x &= (\rho_{34} + \rho_{43})/2, \\ n_e &= (\rho_{11} + \rho_{22})/2, & n_T &= (\rho_{33} + \rho_{44})/2, \end{aligned} \quad (18)$$

where $S_{x,y,z}$ and $J_{x,y,z}$ are the components of the electron and trion spin polarization. n_e and n_T are the populations of the electron and trion states.

After the excitation pulse the spin dynamics of the trion in magnetic field is given by[33]:

$$J_z(t) = J_z^a e^{-(t-t_0)/\tau_T}, \quad J_y(t) = J_y^a e^{-(t-t_0)/\tau_T}, \quad J_x(t) = J_x^a e^{-(t-t_0)/\tau_T}, \quad (19)$$

Here τ_T is the trion spin lifetime, $1/\tau_T \equiv 1/T_s^h + 1/\tau_r$.

The electron spin components after the pulse are:

$$\begin{aligned} S_z(t) &= e^{-(t-t_0)/T_2^e} [(S_z^a + \xi_1 J_z^a) \cos(\omega_L(t-t_0)) + (S_y^a + \xi_2 J_z^a) \sin(\omega_L(t-t_0))] - J_z^a \xi_1 e^{-(t-t_0)/\tau_T} \\ S_y(t) &= e^{-(t-t_0)/T_2^e} [-(S_z^a + \xi_1 J_z^a) \sin(\omega_L(t-t_0)) + (S_y^a + \xi_2 J_z^a) \cos(\omega_L(t-t_0))] - J_z^a \xi_2 e^{-(t-t_0)/\tau_T} \\ S_x(t) &= S_x^a e^{-(t-t_0)/T_1^e}. \end{aligned} \quad (20)$$

Here the superscript a denotes the spin components at time t_0 , when the excitation pulse has passed.

$$\xi_1 + i\xi_2 = \frac{1}{\tau_r(\gamma - i\omega)}, \quad (21)$$

and $\gamma = 1/\tau_T - 1/T_2^e > 0$. The populations n_e and n_T are given by:

$$\begin{aligned} n_T(t) &= n_T^a e^{-(t-t_0)/\tau_r}, \\ n_e(t) &= n_e^a + n_T^a (1 - e^{-(t-t_0)/\tau_r}). \end{aligned} \quad (22)$$

Equations (14) as well as (19), (20), (17) are basis for the following calculations and discussion.

B.4 Optical polarization after the third pulse

In our experiment we measure the amplitude of the electromagnetic wave propagating along the direction $2\mathbf{k}_2 - \mathbf{k}_1$ at delay τ_{12} after the third pulse. This amplitude is determined by the optical polarization created in the sample by all three pulses. The polarization in turn is proportional to the corresponding elements of the density matrix, ρ_{13} , ρ_{24} and c.c. averaged over the ensemble of excited electron-trion systems. At τ_{12} after the third pulse, ρ_{13} and ρ_{24} for the individual systems are given by:

$$\begin{aligned} \rho_{13}(3t_p + 2\tau_{12} + \tau_{23}) &= [\rho_{13}^{a3} \cos(\omega_L \tau_{12}/2) - i\rho_{23}^{a3} \sin(\omega_L \tau_{12}/2)] e^{\tau_{12}(i\omega_0 - 1/T_2)}, \\ \rho_{24}(3t_p + 2\tau_{12} + \tau_{23}) &= [\rho_{24}^{a3} \cos(\omega_L \tau_{12}/2) - i\rho_{14}^{a3} \sin(\omega_L \tau_{12}/2)] e^{\tau_{12}(i\omega_0 - 1/T_2)}. \end{aligned} \quad (23)$$

To obtain the macroscopic polarization one has to average these expressions for an individual electron-trion system over the trion resonance frequency ω_0 . It is obvious, that the condition for observing a stimulated photon echo signal is excluding the factor $e^{i\omega_0\tau_{12}}$ from Eq. (23). As it will be shown below, this is possible because some contributions to ρ_{13}^{a3} , ρ_{23}^{a3} , ρ_{24}^{a3} , ρ_{14}^{a3} contain $e^{-i\omega_0\tau_{12}}$. We turn now to step-by-step calculations of ρ_{13} and ρ_{24} from Eq. (23).

Before excitation with the first pulse only elements of the density matrix describing the electron are unequal to zero (see Eq. 12). We also assume, that these non-zero elements are only populations ρ_{11} and ρ_{22} , $\rho_{11} = \rho_{22} = 1/2$.

1. *The first pulse* changes electron and trion populations and creates optical polarization, that is proportional to the elements ρ_{13} , ρ_{24} and c.c.

$$\begin{aligned}\rho_{13}^{a1} &= i\theta_{1+}e^{i(\omega t_p - \mathbf{k}_1 \mathbf{r})}/4, & \rho_{31}^{a1} &= -i\theta_{1+}e^{-i(\omega t_p - \mathbf{k}_1 \mathbf{r})}/4, \\ \rho_{24}^{a1} &= i\theta_{1-}e^{i(\omega t_p - \mathbf{k}_1 \mathbf{r})}/4, & \rho_{42}^{a1} &= -i\theta_{1-}e^{-i(\omega t_p - \mathbf{k}_1 \mathbf{r})}/4.\end{aligned}\quad (24)$$

Here the superscript ‘a1’ indicates the values after the first pulse action.

2. At the moment of *the second pulse* arrival these elements, ρ_{13} , ρ_{24} and c.c., (and also those arising in magnetic field ρ_{14} , ρ_{32} and c.c.) - in contrast to other elements - contain the phase factor $\exp(\pm i\omega_0\tau_{12})$, see Eqs. (14). For distinctness, the nondiagonal elements, which are proportional to $\exp(-i\omega_0\tau_{12})$, are given by:

$$\begin{aligned}\rho_{31}^{b2} &= -i\theta_{1+}e^{-i(\omega t_p + \omega_0\tau_{12} - \mathbf{k}_1 \mathbf{r})} \cos(\omega_L\tau_{12}/2)e^{-\tau_{12}/T_2}/4, \\ \rho_{32}^{b2} &= \theta_{1+}e^{-i(\omega t_p + \omega_0\tau_{12} - \mathbf{k}_1 \mathbf{r})} \sin(\omega_L\tau_{12}/2)e^{-\tau_{12}/T_2}/4, \\ \rho_{42}^{b2} &= -i\theta_{1-}e^{-i(\omega t_p + \omega_0\tau_{12} - \mathbf{k}_1 \mathbf{r})} \cos(\omega_L\tau_{12}/2)e^{-\tau_{12}/T_2}/4, \\ \rho_{41}^{b2} &= \theta_{1-}e^{-i(\omega t_p + \omega_0\tau_{12} - \mathbf{k}_1 \mathbf{r})} \sin(\omega_L\tau_{12}/2)e^{-\tau_{12}/T_2}/4.\end{aligned}\quad (25)$$

The superscript ‘b2’ indicates that these values are before the second pulse coming in.

3. The action of *the second pulse*, together with the already existing optical polarization of the electron-trion system, leads to additions to populations ρ_{11}^{a2} , ρ_{22}^{a2} , ρ_{33}^{a2} , ρ_{44}^{a2} and spin coherences ρ_{12}^{a2} , ρ_{34}^{a2} , which are proportional to $\exp(-i\omega_0\tau_{12})$. For convenience we rewrite these elements of the density matrix through the components of the electron and trion spin polarizations and populations.

$$\begin{aligned}S_z^{a2} &\sim -K\Delta \cos(\omega_L\tau_{12}/2), & S_y^{a2} &\sim K\Delta \sin(\omega_L\tau_{12}/2), & S_x^{a2} &\sim -iK\Sigma \sin(\omega_L\tau_{12}/2), \\ J_z^{a2} &\sim K\Delta \cos(\omega_L\tau_{12}/2), & J_y^{a2} &\sim -K\Delta_T \sin(\omega_L\tau_{12}/2), & J_x^{a2} &\sim iK\Sigma_T \sin(\omega_L\tau_{12}/2), \\ n_e^{a2} &\sim -2K\Sigma \cos(\omega_L\tau_{12}/2), & n_T^{a2} &\sim 2K\Sigma \cos(\omega_L\tau_{12}/2),\end{aligned}\quad (26)$$

where

$$\begin{aligned}K &= \frac{1}{16}e^{-i(\omega t_p + \omega_0\tau_{12} - \mathbf{k}_1 \mathbf{r} + \mathbf{k}_2 \mathbf{r})}e^{-\tau_{12}/T_2}, \\ \Delta &= \theta_{1+}\theta_{2+} - \theta_{1-}\theta_{2-}, & \Sigma &= \theta_{1+}\theta_{2+} + \theta_{1-}\theta_{2-}, \\ \Delta_T &= \theta_{1+}\theta_{2-} - \theta_{1-}\theta_{2+}, & \Sigma_T &= \theta_{1+}\theta_{2-} + \theta_{1-}\theta_{2+}.\end{aligned}\quad (27)$$

4. Before *the third pulse arrival* the elements $\rho_{11}^{b3}, \rho_{33}^{b3}, \rho_{22}^{b3}, \rho_{44}^{b3}, \rho_{12}^{b3}, \rho_{34}^{b3}$, which correspond to spin populations and spin coherences, contain only a phase factor with optical frequency $\exp(\pm i\omega_0\tau_{12})$, which arose from the second pulse action. Spin dynamics and relaxation after the second pulse result in Larmor precession and decay (see Eqs. (19), (20)). The other elements contain phase factors such as $\exp(\pm i\omega_0\tau_{23}), \exp(\pm i\omega_0(\tau_{23} \pm \tau_{12}))$. It should be noted, that if $\tau_{23} \gg T_2$ and $\tau_{23} \gg \tau_r$ then only electron spin coherence and populations can contribute to the echo signal.

The trion spin polarization shortly before the third pulse is given by:

$$\begin{aligned} J_z^{b3} &\sim K\Delta e^{-\tau_{23}/\tau_T} \cos(\omega_L\tau_{12}/2), & J_y^{b3} &\sim -K\Delta_T e^{-\tau_{23}/\tau_T} \sin(\omega_L\tau_{12}/2), \\ J_x^{b3} &\sim iK\Sigma_T e^{-\tau_{23}/\tau_T} \sin(\omega_L\tau_{12}/2), \end{aligned} \quad (28)$$

where as the electron spin polarization is given by:

$$\begin{aligned} S_z^{b3} &\sim K\Delta \left[e^{-\tau_{23}/T_2^e} [(-1 + \xi_1) \cos(\omega_L\tau_{12}/2) \cos(\omega_L\tau_{23}) + \right. \\ &\quad \left. + (\sin(\omega_L\tau_{12}/2) + \xi_2 \cos(\omega_L\tau_{12}/2)) \sin(\omega_L\tau_{23})] - e^{-\tau_{23}/\tau_T} \xi_1 \cos(\omega_L\tau_{12}/2) \right], \\ S_y^{b3} &\sim K\Delta \left[e^{-\tau_{23}/T_2^e} [(1 - \xi_1) \cos(\omega_L\tau_{12}/2) \sin(\omega_L\tau_{23}) + \right. \\ &\quad \left. + (\sin(\omega_L\tau_{12}/2) + \xi_2 \cos(\omega_L\tau_{12}/2)) \cos(\omega_L\tau_{23})] - e^{-\tau_{23}/\tau_T} \xi_2 \cos(\omega_L\tau_{12}/2) \right], \\ S_x^{b3} &\sim -iK\Sigma e^{-\tau_{23}/T_1^e} \sin(\omega_L\tau_{12}/2). \end{aligned} \quad (29)$$

Further, the populations n_e and n_T read:

$$\begin{aligned} n_e^{b3} &\sim -2K\Sigma e^{-\tau_{23}/\tau_r} \cos(\omega_L\tau_{12}/2), \\ n_T^{b3} &\sim 2K\Sigma e^{-\tau_{23}/\tau_r} \cos(\omega_L\tau_{12}/2) \end{aligned} \quad (30)$$

5. The amplitude of the stimulated photon echo is proportional to the optical polarizations terms ρ_{13} and ρ_{24} after *the third pulse arrival* at $t = 3t_p + 2\tau_{12} + \tau_{23}$.

$$\begin{aligned} \rho_{13}(3t_p + 2\tau_{12} + \tau_{23}) &= -\frac{i}{2} e^{i(\omega t_p + \omega_0\tau_{12} - \mathbf{k}\mathbf{3r})} e^{-\tau_{12}/T_2} \times \\ &\quad \left[\theta_{3+} \left(\frac{n_T^{b3} - n_e^{b3}}{2} + J_z^{b3} - S_z^{b3} \right) \cos(\omega_L\tau_{12}/2) + (\theta_{3-} (J_y^{b3} - iJ_x^{b3}) - \theta_{3+} (S_y^{b3} - iS_x^{b3})) \sin(\omega_L\tau_{12}/2) \right] \\ \rho_{24}(3t_p + 2\tau_{12} + \tau_{23}) &= -\frac{i}{2} e^{i(\omega t_p + \omega_0\tau_{12} - \mathbf{k}\mathbf{3r})} e^{-\tau_{12}/T_2} \times \\ &\quad \left[\theta_{3-} \left(\frac{n_T^{b3} - n_e^{b3}}{2} - J_z^{b3} + S_z^{b3} \right) \cos(\omega_L\tau_{12}/2) + (-\theta_{3+} (J_y^{b3} + iJ_x^{b3}) + \theta_{3+} (S_y^{b3} + iS_x^{b3})) \sin(\omega_L\tau_{12}/2) \right] \end{aligned} \quad (31)$$

B.5 Stimulated photon echo amplitude

Our analysis shows that the choice of the polarization configuration for the excitation pulses gives us flexibility for observing different mechanisms of photon echo generation. There are two radically different configurations: (i) all pulses are linearly co-polarized, for example, horizontally (HHH) and (ii) the first and the second pulses are linearly cross-polarized. For clarity we will discuss configuration HVV in the following. One can rewrite Eqs. (31) for these two configurations.

B.5.1 Configuration HHH

In this case $\theta_{1+} = \theta_{1-} \equiv \theta_1$, $\theta_{2+} = \theta_{2-} \equiv \theta_2$, and $\theta_{3+} = \theta_{3-} \equiv \theta_3$. This leads to $\Delta = \Delta_T = 0$, $\Sigma = \Sigma_T = 2\theta_1\theta_2$, and, therefore, $S_z = S_y = J_z = J_y = 0$. The polarization of the stimulated echo signal is also horizontal:

$$P_{HHHH} \sim -ie^{i(\omega t_p + \omega_0 \tau_{12} - \mathbf{k}_3 \mathbf{r})} e^{-\tau_{12}/T_2} \theta_3 \times \left[\frac{n_T^{b3} - n_e^{b3}}{2} \cos(\omega_L \tau_{12}/2) - i(J_x^{b3} - S_x^{b3}) \sin(\omega_L \tau_{12}/2) \right] + c.c. \quad (32)$$

From this equation it is obvious, that only one term of this expression, namely the one which is proportional to S_x^{b3} decays exponentially with the long relaxation time of the electron spin, T_1^e , when we increase the delay between the second and the third pulses τ_{23} . The other terms, which are proportional to n_T^{b3} , n_e^{b3} and J_x^{b3} , decay on the shorter time scales τ_r or τ_T . One can also clearly see that the long-lived part appears exclusively in magnetic field.

If we rewrite the previous equation with substitution of all terms, we obtain:

$$P_{HHHH} \sim -\frac{i}{8} e^{i(\mathbf{k}_1 - \mathbf{k}_2 - \mathbf{k}_3) \mathbf{r}} e^{-2\tau_{12}/T_2} \theta_1 \theta_2 \theta_3 \times \left[e^{-\tau_{23}/\tau_r} (2 \cos^2(\omega_L \tau_{12}/2) + e^{-\tau_{23}/T_h} \sin^2(\omega_L \tau_{12}/2)) + e^{-\tau_{23}/T_1^e} \sin^2(\omega_L \tau_{12}/2) \right] + c.c. \quad (33)$$

The long-lived part is expected to show up as a constant background at fixed magnetic field, when the stimulated echo is measured as function of τ_{23} , or as slowly oscillating background when the echo is measured as function of magnetic field.

B.5.2 Configuration HVV

In this configuration $\theta_{1+} = \theta_{1-} \equiv \theta_1$, $\theta_{2+} = -\theta_{2-} \equiv \theta_2$, $\theta_{3+} = -\theta_{3-} \equiv \theta_3$. This leads to $\Delta = -\Delta_T = 2\theta_1\theta_2$ and $\Sigma = \Sigma_T = 0$.

The polarization of the stimulated echo signal is horizontal:

$$P_{HVVH} \sim -ie^{i(\omega t_p + \omega_0 \tau_{12} - \mathbf{k}_3 \mathbf{r})} e^{-\tau_{12}/T_2} \theta_3 \times \left[(J_z^{b3} - S_z^{b3}) \cos(\omega_L \tau_{12}/2) - (J_y^{b3} + S_y^{b3}) \sin(\omega_L \tau_{12}/2) \right] + c.c. \quad (34)$$

Clearly this signal contains long-lived and short-lived parts. After substitution of $S_{z,y}^{b3}$ and $J_{z,y}^{b3}$, we obtain:

$$P_{HVVH} \sim -\frac{i}{8} e^{i(\mathbf{k}_1 - \mathbf{k}_2 - \mathbf{k}_3) \mathbf{r}} e^{-2\tau_{12}/T_2} \theta_1 \theta_2 \theta_3 \times \left[e^{-\tau_{23}/\tau_T} (\cos(\omega_L \tau_{12}) + \cos(\omega_L \tau_{12}/2) [\xi_1 \cos(\omega_L \tau_{12}/2) + \xi_2 \sin(\omega_L \tau_{12}/2)]) + e^{-\tau_{23}/T_2^e} [\cos(\omega_L (\tau_{12} + \tau_{23})) - \cos(\omega_L \tau_{12}/2) [\xi_1 \cos(\omega_L (\tau_{12}/2 + \tau_{23})) + \xi_2 \sin(\omega_L (\tau_{12}/2 + \tau_{23}))]] \right] + c.c. \quad (35)$$

If trion spin relaxes before trion recombination, $T_h \ll \tau_r$, then $\xi_1 = \xi_2 = 0$ and P_{HVVH} :

$$P_{HVVH} \sim -\frac{i}{8} e^{i(\mathbf{k}_1 - \mathbf{k}_2 - \mathbf{k}_3) \mathbf{r}} e^{-2\tau_{12}/T_2} \theta_1 \theta_2 \theta_3 \times \left[e^{-\tau_{23}/\tau_T} \cos(\omega_L \tau_{12}) + e^{-\tau_{23}/T_2^e} \cos(\omega_L (\tau_{12} + \tau_{23})) \right] + c.c. \quad (36)$$

One sees from this equation, that the amplitude of the long-lived signal at zero magnetic field and the amplitude of the long-lived oscillations in magnetic field are the same. If we sum P_{HVVH} over all ω_L to take into account a possible spread of Larmor frequencies, then the oscillating signal in magnetic field can decay faster than the signal in zero magnetic field.

If the trion spin relaxes slowly, $T_h \gg \tau_r$, then the amplitude of the long-lived signal depends strongly on magnetic field. In zero magnetic field P_{HVVH} is:

$$P_{HVVH} \sim -\frac{i}{8} e^{i(\mathbf{k}_1 - \mathbf{k}_2 - \mathbf{k}_3)\mathbf{r}} e^{-2\tau_{12}/T_2} \theta_1 \theta_2 \theta_3 \times \left[e^{-\tau_{23}/\tau_T} (1 + \xi_1) + e^{-\tau_{23}/T_2^e} (1 - \xi_1) \right] + c.c. \quad (37)$$

The long-lived part of the signal is proportional to $1 - \xi_1 \approx \tau_r/(T_h + \tau_r)$, therefore if $T_h \gg \tau_r$, then the signal at $B = 0$ vanishes. This is due to the fact that after the second pulse a long-lived spin polarization S , which is responsible for the long-lived echo signal, does not appear: after trion recombination the spin state of the resident carrier does not differ from that before trion formation.

In a transverse magnetic field the change of the relative orientation of the electron spin and the trion spin leads to appearance of spin polarization of the resident electrons, even if the spins of the carriers in the trions do not relax [33]. With increasing magnetic field this imbalance leads to an increase of the stimulated photon echo amplitude.

B.5.3 Stimulated photon echo before the first pulse arrival

It is worth recalling that all pulses in our experiment arrive periodically with the laser repetition period $T_R \approx 13$ ns. The stimulated photon echo signal before the first pulse arrival (see Fig. 3) is in fact the signal created by the preceding pair of pulses 1 and 2. At τ_{23} close to T_R changes of the initial conditions for ρ by the third pulse before the arrival of the first pulse have to be taken into account. For the configurations with linearly polarized pulses we have to consider only changes of n_e and n_T induced by the previous three pulses, because the other components of spin or polarization contain phase factors and do not contribute to the signal. If τ_{23} close to T_R , n_e and n_T are changed only by the third pulse then. As a result, the density matrix before the subsequent first pulse arrival is given by:

$$\rho^{b1} = \frac{1}{2} \begin{pmatrix} n_e^{b1} & 0 & 0 & 0 \\ 0 & n_e^{b1} & 0 & 0 \\ 0 & 0 & n_T^{b1} & 0 \\ 0 & 0 & 0 & n_T^{b1} \end{pmatrix}. \quad (38)$$

Here $n_T^{b1} = \theta_3^2 e^{-\tau_{31}/\tau_r} / 4$, $n_e^{b1} = 1 - \theta_3^2 e^{-\tau_{31}/\tau_r} / 4$, τ_{31} is the temporal separation between the third pulse and the next first pulse, $\tau_{31} = T_R - (\tau_{12} + \tau_{23})$.

These initial conditions lead for the signals P_{HHHH} and P_{HVVH} only to one additional factor $\sim (n_e^{b1} - n_T^{b1}) = 1 - \theta_3^2 e^{-\tau_{31}/\tau_r} / 2$. This factor corresponds to an exponential decrease of the echo signal at negative delay τ_{23} close to the first pulse. In our case this decrease can be seen in P_{HHHH} through the long-lived component of the signal in magnetic field, which still exists in the relevant temporal range as it does not decay due to a Larmor frequency spread so that it is preserved until the next first pulse arrival.

References and Notes

- [1] Kurnit, N. A., Abella, I. D. & Hartmann, S. R. Observation of a photon echo. *Phys. Rev. Lett.* **13**, 567-568 (1964).
- [2] Mossberg, T., Flusberg, A., Kachru, R. & Hartmann, S. R. Total scattering cross section for Na on He measured by stimulated photon echoes. *Phys. Rev. Lett.* **42**, 1665-1669 (1979).
- [3] Takeuchi, N. & Szabo, A. Observation of photon echoes using a nitrogen laser pumped dye laser. *Phys. Lett. A* **50**, 361-362 (1974).
- [4] Noll, G., Siegner, U., Schevel, S. G. & Göbel, E. O. Picosecond stimulated photon echo due to intrinsic excitations in semiconductor mixed crystals. *Phys. Rev. Lett.* **64**, 792-795 (1990).
- [5] Webb, M. D., Cundiff, S. T. & Steel, D. G. Observation of time-resolved picosecond stimulated photon echoes and free polarization decay in GaAs/AlGaAs multiple quantum wells. *Phys. Rev. Lett.* **66**, 934-937 (1991).
- [6] Wiersma, D. A. & Duppen, K. Picosecond holographic-grating spectroscopy. *Science* **237**, 1147-1154 (1987).
- [7] Chemla, D. S. & Shah, J. Many-body and correlation effects in semiconductors. *Nature* **411**, 549-557 (2001).
- [8] Samartsev, V. V. Coherent optical spectroscopy of promising materials for solid-state optical processors. *Laser Physics* **20**, 383-446 (2010).
- [9] Lvovsky, A. I., Sanders, B. C. & Tittel, W. Optical quantum memory. *Nature Photonics* **3**, 706-714 (2009).
- [10] Hammerer, K., Sørensen, A. S. & Polzik, E. S. Quantum interface between light and atomic ensembles. *Rev. Mod. Phys.* **82**, 1041-1093 (2010).
- [11] Lambert, L. Q., Compaan, A. & Abella, I. D. Modulation and fast decay of photon-echos in ruby. *Physics Letters A* **30**, 153-154 (1969).
- [12] Chen, Y. C., Chiang, K. & Hartmann, S. R. Photon echo relaxation in $\text{LaF}_3\text{:Pr}^{3+}$. *Optics Communications* **29**, 181-185 (1979).
- [13] Morsink, J. B. S., Hesselink, W. H. & Wiersma, D. A. Photon echo stimulated from optically induced nuclear spin polarization. *Chem. Phys. Lett.* **64**, 1-4 (1979).
- [14] Alekseev, A. I., Basharov, A. M. & Beloborodov, V. N. Photon-echo quantum beats in a magnetic field. *J. Phys. B: At. Mol. Phys.* **16**, 4697-4715 (1983).

- [15] Rubtsova, N. N., Ishchenko, V. N., Khvorostov, E. B., Kochubei, S. A., Reshetov, V. A. & Yevseyev, I. V. Non-Faraday rotation of photon-echo polarization in ytterbium vapor. *Phys. Rev. A* **70**, 023403 (2004).
- [16] Langer, L., Poltavtsev, S. V., Yugova, I. A., Yakovlev, D. R., Karczewski, G., Wojtowicz, T., Kossut, J., Akimov, I. A. & Bayer, M. Magnetic-field control of photon echo from the electron-trion system in a CdTe quantum well: Shuffling coherence between optically accessible and inaccessible states. *Phys. Rev. Lett.* **109**, 157403 (2012).
- [17] Afzelius, M., Usmani, I., Amari, A., Lauritzen, B., Walther, A., Simon, C., Sangouard, N., Minář, J., de Riedmatten, H., Gisin, N. & Kröll, S. Demonstration of atomic frequency comb memory for light with spin-wave storage. *Phys. Rev. Lett.* **104**, 040503 (2010).
- [18] Greilich, A., Yakovlev, D. R., Shabaev, A., Efros, A. L., Yugova, I. A., Oulton, R., Stavarache, V., Reuter, D., Wieck, A. & Bayer, M. Mode locking of electron spin coherences in singly charged quantum dots. *Science* **313**, 341-345 (2006).
- [19] Press, D., Ladd, T. D., Zhang B. & Yamamoto, Y. Complete quantum control of a single quantum dot spin using ultrafast optical pulses. *Nature* **456**, 218-221 (2008).
- [20] Berezovsky, J., Mikkelsen, M. H., Stoltz, N. G., Coldren, L. A. & Awschalom, D. D. Picosecond coherent optical manipulation of a single electron spin in a quantum dot. *Science* **320**, 349-352 (2008).
- [21] Xu, X., Sun, B., Berman, P. R., Steel, D. G., Bracker, A. S., Gammon, D. & Sham, L. J. Coherent population trapping of an electron spin in a single negatively charged quantum dot. *Nature Physics* **4**, 692-695 (2008).
- [22] Zhukov, E. A., Yakovlev, D. R., Bayer, M., Glazov, M. M., Ivchenko, E. L., Karczewski, G., Wojtowicz, T. & Kossut, J. Spin coherence of a two-dimensional electron gas induced by resonant excitation of trions and excitons in CdTe/(Cd,Mg)Te quantum wells. *Phys. Rev. B* **76**, 205310 (2007).
- [23] Also localization of an electron at a donor located in QW is possible. In this case optical transitions between donor bound electron and donor bound exciton (D^0X) are addressed. Most importantly, however, the same SPE scenarios are valid for the trion and donor-bound exciton complexes.
- [24] Note that the density of electrons in the QW is low (exciton Bohr radius $a_B \ll \sqrt{n_e}$), which allows us to consider the resident electrons as isolated, non-interacting carriers. Many-body interactions are weak and can be neglected at the low excitation densities used in our experiment (pulse energies below 100 nJ cm^{-2}).
- [25] For the neutral exciton the transitions at zero magnetic field are not circularly but linearly polarized. Moreover, in magnetic field the exciton level splitting is determined by electron and hole Zeeman splitting, and not only by the hole one.

- [26] Debus, J., Dunker, D., Sapega, V.F., Yakovlev, D.R., Karczewski, G., Wojtowicz, T., Kosut, J. & Bayer, M. Spin-flip Raman scattering of the neutral and charged excitons confined in a CdTe/(Cd,Mg)Te quantum well. *Phys. Rev. B* **87**, 205316 (2013).
- [27] Zrenner, A., Beham, E., Stufliker, S., Findeis, F., Bichler, M. & Abstreiter, G. Coherent properties of a two-level system based on a quantum-dot photodiode. *Nature* **418**, 612-614 (2002).
- [28] Kroutvar, M., Ducommun, Y., Heiss, D., Bichler, M., Schuh, D., Abstreiter, G. & Finley, J.J. Optically programmable electron spin memory using semiconductor quantum dots. *Nature* **432**, 81-84 (2004).
- [29] Oulton, R., Greilich, A., Verbin, S.Yu., Cherbunin, R. V., Auer, T., Yakovlev, D.R., Bayer, M., Merkulov, I. A., Stavarache, V., Reuter, D. & Wieck, A. D. Subsecond spin relaxation times in quantum dots at zero applied magnetic field due to a strong electron-nuclear interaction. *Phys. Rev. Lett.* **98**, 107401 (2007).
- [30] Langbein W. & Borri P. *Semiconductor Qubits* edited by F. Henneberger and O. Benson, Ch. 12, p. 269 (Pan Stanford Publishing, Singapore, 2008).
- [31] E. L. Ivchenko, *Optical Spectroscopy of Semiconductor Nanostructures* (Alpha Science, Harrow UK, 2005).
- [32] I. A. Yugova, M. M. Glazov, E. L. Ivchenko, and A. L. Efros, *Phys. Rev. B* **80**, 104436 (2009).
- [33] I. A. Yugova, M. M. Glazov, D. R. Yakovlev, A. A. Sokolova, and M. Bayer, *Phys. Rev. B* **85**, 125304 (2012).

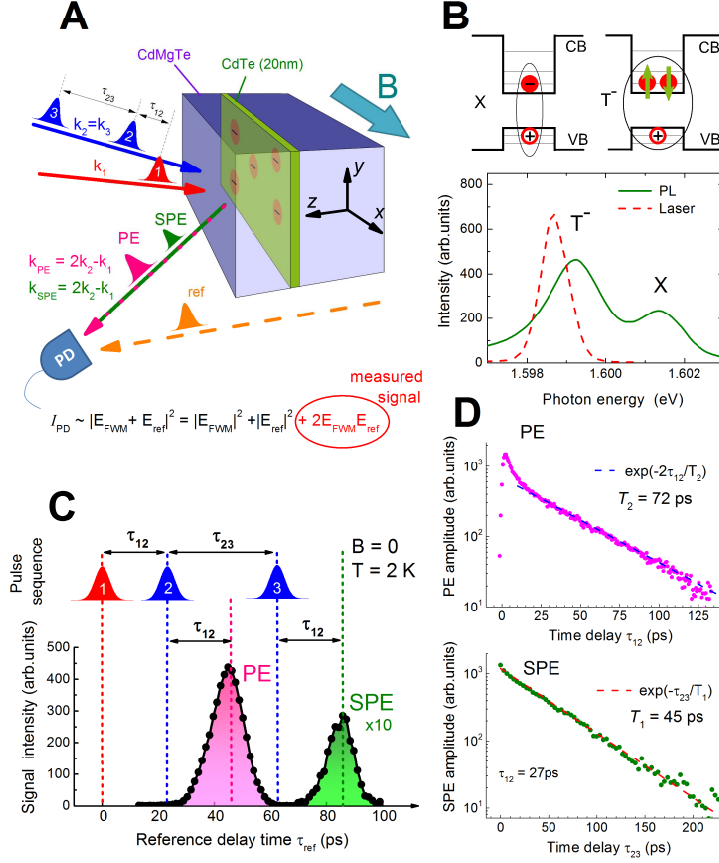


Fig. 1. Scheme of photon echo experiment and optical properties of investigated structure. (A) The CdTe/(Cd,Mg)Te quantum well (QW) is optically excited with a sequence of three laser pulses with variable delays τ_{12} and τ_{23} relative to each other. The resulting four-wave mixing transients $|E_{FWM}(t)|$ are detected in $2\mathbf{k}_2 - \mathbf{k}_1$ direction using heterodyne detection. All measurements are performed at temperature of 2 K. (B) Top: schematic presentation of exciton (X) and trion (T^-) complexes in QW. The QW potential of conduction (CB) and valence (VB) bands leads to spatial trapping of electrons and holes. Bottom: Photoluminescence (PL) spectrum (solid line) measured for above-barrier excitation with photon energy 2.33 eV, demonstrating X and T^- emission. The laser spectrum (dashed line) used in photon echo experiment is tuned to the low energy flank of T^- emission line. (C) Four-wave mixing transients for $\tau_{12} = 23$ ps and $\tau_{23} = 39$ ps. Spontaneous (PE) and stimulated (SPE) photon echo signals appear at $\tau_{ref} = 2\tau_{12}$ and $\tau_{ref} = 2\tau_{12} + \tau_{23}$, respectively. (D) Decay of PE and SPE peak amplitudes. From exponential fits (dashed lines) we evaluate $T_2 = 72$ ps and $T_1 = 45$ ps.

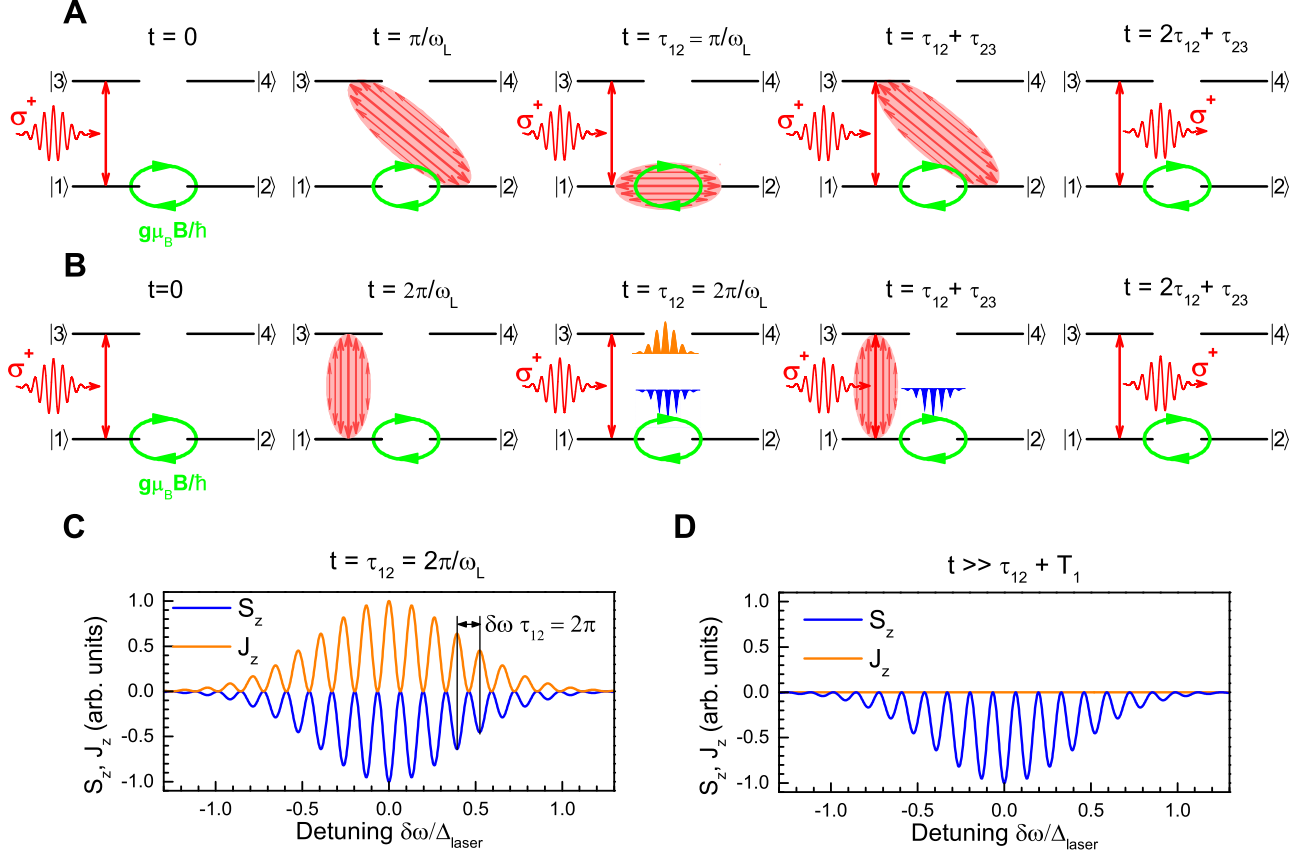


Fig. 2. Schematic presentation of the main mechanisms responsible for magnetic-field-induced stimulated photon echoes (SPE). Optical pulses are circularly polarized. (A) Transfer of optical coherence into electron spin coherence (S_x and S_y components). The efficiency is maximum for $\tau_{12} = \pi/\omega_L$. (B) Creation of spectral spin fringes for electrons and trions (S_z and J_z components). This mechanism is most efficient for $\tau_{12} = 2\pi/\omega_L$. The spectral spin gratings for electrons and trions are shown in (C) at the moment of creation by the second pulse ($t = \tau_{12} = 2\pi/\omega_L$) and in (D) after trion recombination and before arrival of pulse 3 ($t \gg \tau_{12} + T_1$).

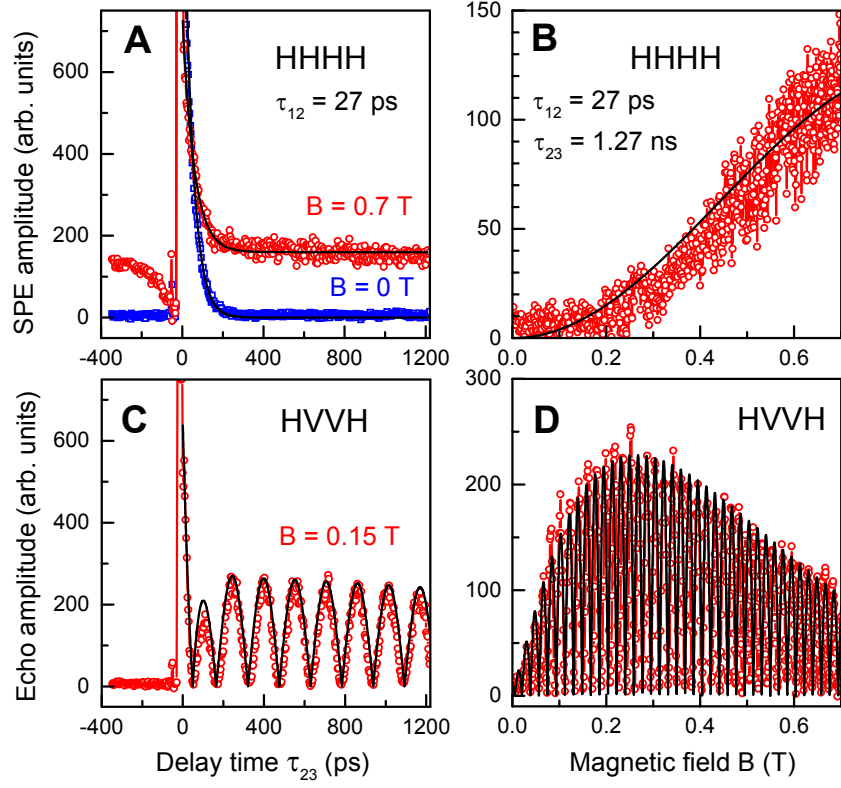


Fig. 3. Experimental demonstration of magnetic-field-induced long-lived stimulated photon echo (SPE). The delay time τ_{12} is set to 27 ps. (A) Stimulated echo amplitude in configuration HHHH as function of time delay τ_{23} at $B = 0$ and 0.7 T. (B) Long-lived part of the stimulated echo amplitude as function of magnetic field. Dots are experimental data. Black curves in A and B give theoretical calculations with parameters: $g = 1.52$, $\tau_r = 43$ ps, $T_h = 1000$ ps, and $T_1^e \sim 50$ ns. (C) Stimulated echo amplitude in configuration HVVH as function of the delay τ_{23} at $B = 0.15$ T. (D) Long-lived part of stimulated echo amplitude versus magnetic field. Black curves in C and D are calculations with parameters: $g = 1.52$, $\Delta g = 0.018$, $\tau_r = 43$ ps, $T_h = 1000$ ps, and $T_2^e > T_R$.